PERGAMON

Continental Shelf Research 21 (2001) 697–725

CONTINENTAL SHELF RESEARCH

www.elsevier.com/locate/csr

Weak wave–tide interaction formulation and its application to Cádiz bay

B.A. Kagan[a,b,*], L. Tejedor[a], O. Álvarez[a], A. Izquierdo[a], B. Tejedor[a], R. Mañanes[a]

[a] *Departamento de Física Aplicada, Universidad de Cádiz, Cádiz, Spain*

[b] *Shirshov Institute of Oceanology, Russian Academy of Sciences, St. Petersburg Branch, St. Petersburg, Russia*

Received 8 July 1999; accepted 5 June 2000

Abstract

Using a single-point, one-equation (k–l) model for an oscillatory turbulent bottom boundary layer (BBL) above a hydrodynamically rough bottom and varying the external determining parameters over a wide range, we show that nonlinear wave/low-frequency current interaction effects are smaller, the greater are the ratio of near-bottom wave orbital velocity amplitude to friction-free, low-frequency current velocity amplitude and the ratio between frequencies of wave and low-frequency components of motion. Specifically, in shallow waters the bottom stress oscillations with wave and tidal frequencies are, with fair accuracy, weakly correlated, thereby suggesting that wave-tide interaction is substantially weak interaction. A new weak wave–tide interaction formulation is proposed. It involves a relationship for the drag coefficient in a wave-affected tidal flow and the surface Rossby number dependences for the scaled wave and tidal friction velocity amplitudes inferred from the resistance law for an oscillatory turbulent BBL over a hydrodynamically rough surface. This formulation is implemented within a 2D nonlinear, finite-difference, high-resolution, hydrodynamic model and the modified model is applied to quantify the wave-induced changes in the tidal dynamics and energetics of Cádiz Bay. The model results reveal one unexpected feature in the fields of maximum tidal velocity and mean tidal energy flux. Namely, wave–tide interaction responsible for enhancing the mean bottom stress throughout the bay tends to increase the maximum tidal velocities and the mean tidal energy fluxes at deeper depths and to reduce them at shallower depths. The reason for appearing this feature is an overall amplification of the mean tidal energy transport into the bay from Gulf of Cádiz. Based on the sensitivity study to varying wave parameters, the wave-induced seasonal variability in the M_2 tidal characteristics is found to be not pronounced in Cádiz Bay. This, however, does not rule out a clearly defined manifestation of such a variability in other shallow basins

*Corresponding author. Tel./fax: +34-956-470-866.

E-mail address: oscar.alvarez@uca.es (O. Álvarez).

PII: S0278-4343(00)00099-6

and/or in other tidal frequency bands. Special attention is given to identify the regions of potential suspended sediment transport and their wave-induced changes.

Keywords: Wave–tide interaction; Tidal dynamics; Energetics; Parameterization; Hydrodynamic model; Cádiz Bay

1. Introduction

At present the most widely used formulation describing the interaction between wind waves and low-frequency motions is the formulation of Grant and Madsen (1979). It has been applied in studies of tides (Davies and Lawrence, 1994a, b; Bender and Wang, 1993), wind-driven circulation (Christoffersen and Jonsson,1985; Signell et al., 1990; Davies and Lawrence, 1995; Davies and Glorioso, 1999), storm surges generated by tropical cyclones (Spaulding and Isaji, 1987; Tang and Grimshaw, 1996), combined tidal and storm-driven flows (Keen and Glenn, 1995) and suspended sediment transport in coastal waters (Lou and Ridd, 1997).

One of the key features of the Grant and Madsen (1979) formulation is related to setting the vertical distribution of the eddy viscosity in the bottom boundary layers (BBLs) for wave and low-frequency motions. The vertical eddy viscosity is specified by a linear function of distance from the bottom with a slope of von Karman's constant times a combined (wave + low-frequency) bottom friction velocity amplitude in the wave BBL and a low-frequency bottom friction velocity amplitude above the wave BBL. As a result, the vertical velocity shears become discontinuous at the top of and overestimated above the wave BBL. This, in turn, tends to overestimate the effective roughness length.

Another feature concerns the concept of wave/low-frequency current interaction in use. It assumes that both wave and low-frequency bottom friction velocity oscillations are enhanced in the process of their nonlinear interaction and that, hence, the bottom stress in a combined motion of wind waves and low-frequency currents differs from the sum of the bottom stresses produced by purely wave and low-frequency components of motion. Such an interaction may be referred to as strong wave/low-frequency current nonlinear interaction. This concept is inconsistent as it must with data of laboratory and field measurements over a hydrodynamically smooth bottom (Kemp and Simons, 1982; Green et al., 1990). But, what is more important, it is also inconsistent with results of numerical experiments on wave/low-frequency current interaction over a hydrodynamically rough bottom (Davies et al., 1988). This circumstance which has gone unnoticed as well as the intuitive belief that the interaction between motions with widely different spatial and temporal scales can be weak, even though these motions are in themselves strongly nonlinear, call for refining some premises underlying the Grant and Madsen (1979) formulation. By the way, the concept of strong wave/low-frequency current nonlinear interaction has implicitly been revised by Signell et al. (1990), who simplified the Grant and Madsen (1979) formulation assuming that the effect of low-frequency currents on wind waves could be neglected under most conditions. According to Signell et al. (1990), this is because the low-frequency bottom stress significantly affects the wave bottom stress only when the latter is itself negligible compared to the former. In contrast, since the wave

bottom stress in shallow water is much larger than the low-frequency bottom stress, the effect of wind waves on low-frequency currents can be quite significant.

The aim of this paper is four-fold: (1) to clarify, using a single-point, one-equation (k–l) model for an oscillatory turbulent BBL over a hydrodynamically rough bottom, the character of wave/low-frequency current interaction in a wide range of change in the external determining parameters (from 10 to 10^4 for the ratio between frequencies and from 0.5 to 10 for the ratio between friction-free velocity amplitudes of wave and low-frequency motions); (2) to show that wave–tide nonlinear interaction is weak in the sense that the bottom stress oscillations with wave and tidal frequencies may be recognized, with fair accuracy, as weakly correlated and that, hence, a linear superposition of the solutions for purely wave and tidal motions ensures a reasonable accuracy in modelling the BBL characteristics for much of a tidal cycle; (3) to parameterize, from the above reasoning, the influence of wind waves upon tidal dynamics in terms of the drag coefficient in wave-affected tidal flow; and (4) to implement the proposed parameterization within a two-dimensional (2D) in the horizontal, nonlinear, high-resolution, hydrodynamic model and to evaluate, on its basis, the role of wave-tide interaction in the formation of the tidal dynamics and energetics of Cádiz Bay where both the large wind waves and the strong surface tides are well pronounced and where detailed measurements have been made and will continue in the future.

The paper is organized as follows. In the next section we describe briefly the model in use for an oscillatory turbulent BBL over a hydrodynamically rough surface as well as the model results clarifying the character of wave/low-frequency current interaction. In Section 3, the expressions for the drag coefficient and the phase difference between near-bottom velocity and friction-free velocity in a wave-affected tidal flow are given. These expressions contain the unknown ratio of wave friction velocity amplitude to tidal friction velocity amplitude. To determine it, the resistance law for an oscillatory turbulent BBL over a hydrodynamically rough surface is invoked. This law is obtained by matching the asymptotic expansions for velocity amplitudes at small and great heights. In so doing, wave–tide interaction is considered to be weak in the aforementioned sense. Section 4 provides the simulation results with and with no wave–tide interaction effects as applied to the tidal dynamics and energetics of Cádiz Bay. Also presented here are the results of a sensitivity study to varying wind-wave parameters, the results that may help to gain a better understanding of the wave-induced seasonal variability of tidal constants in shallow basins, like Cádiz Bay. The conclusions are drawn in Section 5.

2. Wave–tide interaction: strong or weak?

The answer to the question contained in the title of this section will be provided using a single-point, one-equation, turbulence (k–l) model for an oscillatory turbulent BBL over a hydrodynamically rough surface. Its brief description is given in Appendix A. For more details see Vager and Kagan (1969), Marchuk and Kagan (1977), Johns (1975, 1978), Johns and Oguz (1987) and Davies and Jones (1991).

We now turn to a comparison of the solutions obtained with and with no nonlinear wave/low-frequency current interaction effects (in these cases, the solution is represented either as a general one for a combined wave/low-frequency motion or as a linear superposition of the particular solutions for purely wave and low-frequency motions). To quantify the discrepancies between

Table 1
Relative mean error (E, %) and the correlation coefficient (r) between the bottom stresses predicted with and without nonlinear interaction effects for various values of the ratio of near-bottom wave orbital velocity amplitude to friction-free current velocity amplitude and the ratio of wave frequency to current frequency. Data from Kagan and Utkin (1999)

Amplitude ratio	Frequency ratio							
	10		10^2		10^3		10^4	
	E	r	E	r	E	r	E	r
0.5	63.75	0.4192	51.30	0.6045	2.53	0.9395	0.68	0.9954
1.0	55.65	0.5303	15.88	0.8707	1.46	0.9392	0.11	0.9992
5.0	4.98	0.9517	0.54	0.9949	0.03	0.9997	2×10^{-3}	0.9999
10.0	1.48	0.9853	0.15	0.9985	0.01	0.9999	4×10^{-4}	0.9999

both the solutions we make use of the two parameters: the relative mean (over a low-frequency oscillation cycle) error in the bottom stress values predicted by the solution in the latter case in comparison to those predicted in the former one and the correlation between the two appropriate time series of bottom stress values. The first parameter can serve as a measure of the amplitude difference between the alternative predictions, the second as a measure of the phase difference. The above parameters are presented in Table 1 for various values of the ratio of near-bottom wave orbital velocity amplitude to friction-free, low-frequency current velocity amplitude and the ratio of wave frequency to current frequency. As can be seen, the correlation increases, and the relative mean error decreases with increasing these ratios. Moreover, it turns out that in the case of wave-tide interaction, the case we are interested in, when the velocity amplitude ratio is of the order 1 and the frequency ratio is of the order 10^4, the linear superposition of the solutions for purely wave and tidal flows yields quite plausible results: the relative mean error and the correlation are 0.11% and 0.9992, respectively. The small mean relative error and the high correlation between the solutions obtained with and with no allowance for nonlinear interaction effects means that the bottom stress oscillations with wave and tidal frequencies are in turn weakly correlated suggesting that wave–tide interaction is substantially weak interaction.

An additional point to emphasize is that if one accounts for uncertainties in available experimental data, the accuracy of evaluating the bottom stress by means of the linear superposition of the particular solutions is well higher than that of evaluating the external parameters, especially the bottom roughness length, determining the vertical structure of the BBL. Recall in this connection that the bottom roughness length is determined by the entire spectrum of roughness elements over the area with a linear scale of the order of the bottom logarithmic layer height. The required information about the spatial distribution of roughness elements is generally lacking, so that the bottom roughness length is prescribed either more or less arbitrarily or, in the best case, depending on small-scale bottom topography and bed material composition, according to Heathershaw (1979) results.

The natural question arises: Why does the interaction between wind waves and tidal currents, associated with a drastic intensification of turbulence in the BBL, occur without a marked nonlinear enhancing of the bottom stress? The reason is perhaps that, first, if the gap between the

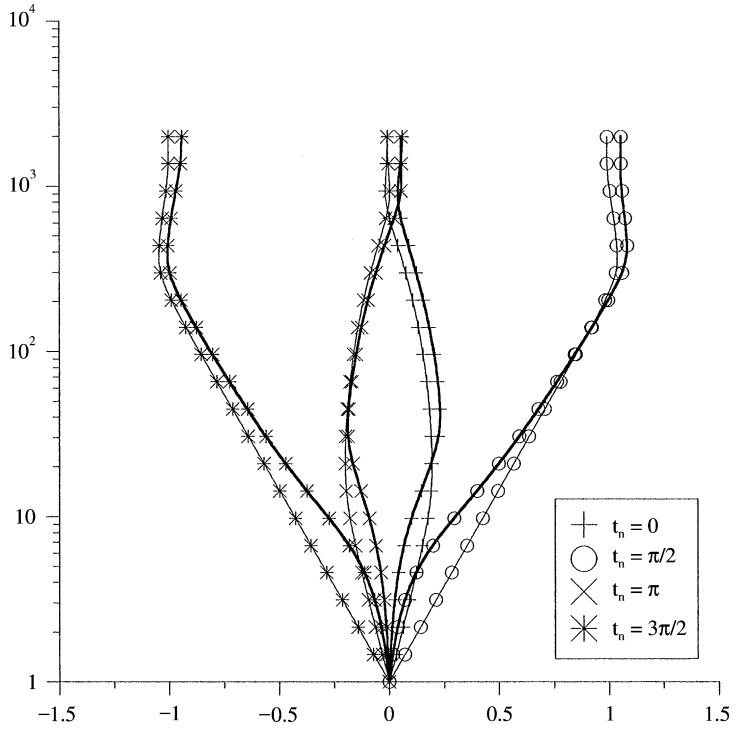

Fig. 1. Wind-wave cycle-averaged vertical velocity profiles in a combined (wave + tide) flow and instantaneous vertical velocity profiles in the relevant purely tidal flow at various times of a tidal cycle. The profiles in the combined and tidal flows are indicated, respectively, by heavy and light lines. Dimensionless heights are plotted on the ordinate, dimensionless velocities are plotted on the abcissa. The normalizing factors for heights and velocities are a bottom roughness length and a friction-free tidal velocity amplitude, respectively; t_n is the dimensionless time defined as $t_n = \sigma_T t$, where σ_T is a tidal frequency.

frequencies of oscillations is wide enough, such oscillations in the process of their nonlinear interaction generate multiple and combinative modes but are in themselves scarcely affected by these modes; and secondly, any changes in the intensity of turbulence are accompanied by opposite changes in the vertical velocity shear, so that their contributions to the bottom stress cancel out. The latter is evident from the comparison of the averaged (over a wind wave cycle) vertical velocity profiles in a combined (wave + tide) flow and the instantaneous vertical velocity profiles in the appropriate purely tidal flow (Fig. 1). This fact by itself is not uninteresting, but in a given case we would like to know how much the instantaneous velocity profiles in the combined flow obtained with and with no allowance for nonlinear interaction effects differ among themselves. The answer to this question is provided by Fig. 2 where the instantaneous vertical velocity profiles for both the solutions are shown. From this figure it follows that the obtained profiles are in close agreement in the near-bottom layer and, generally, throughout the whole BBL at those times of a tidal cycle when the velocity does not change sign.

We call attention to one more remarkable feature of the vertical velocity profiles, namely a decrease in velocity outside the near-bottom logarithmic layer at some times of a tidal cycle. This

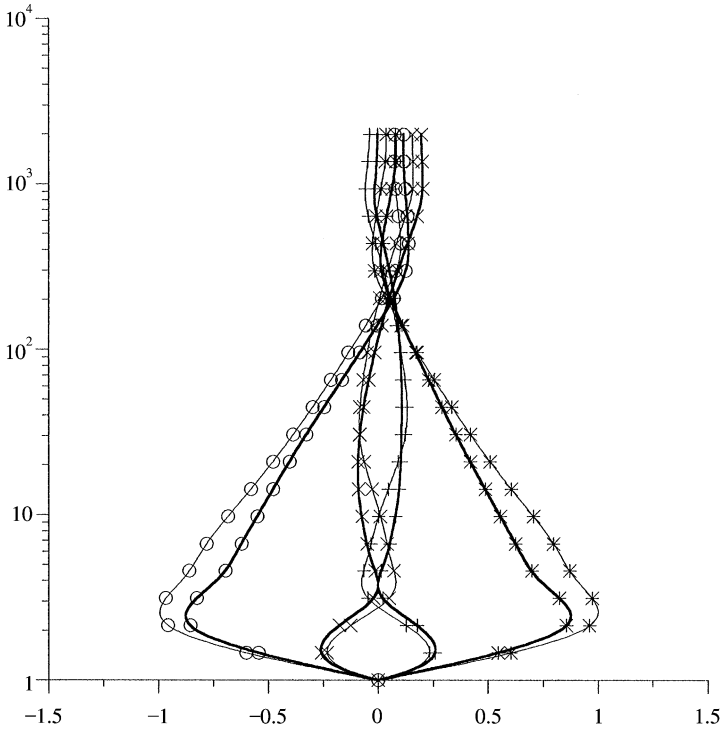

Fig. 2. Instantaneous vertical velocity profiles in a combined flow obtained with (heavy lines) and with no (light lines) nonlinear interaction effects at various times of a tidal cycle. The remaining explanations and, in particular, instants of time these profiles are referred to see Fig. 1.

feature is due to a phase shift between near-bottom wave orbital velocity and friction-free tidal velocity. That such is the case is confirmed by the calculated instantaneous vertical profiles of wave and tidal velocities outlined in Fig. 3.

3. Weak wave–tide interaction formulation

We make use of the model results concerning the logarithmic vertical distribution of velocity and hence a quasi-stationary regime of motion in the near-bottom layer. Further, we assume that (i), because the characteristic time scale of wind waves is much less than the characteristic time scale of tidal currents, the thickness of the wave BBL is much less than the thickness of the tidal BBL; (ii) the influence of wind waves upon tidal dynamics may be described in terms of an effective vertical eddy viscosity; (iii) the latter may be represented as the sum of the two vertical eddy viscosities, each being determined by a certain (wind-wave or tidal) components of motion and is considered to be dependent on the bottom friction velocity amplitude in the appropriate BBL, the assumption of weak wave–tide interaction; and (iv) the effective vertical eddy viscosity is piecewise linear, continuous function of the vertical coordinate. Then the vertical distribution of tidal velocity amplitude, with allowance made for its continuity at the top of the wave BBL, reads

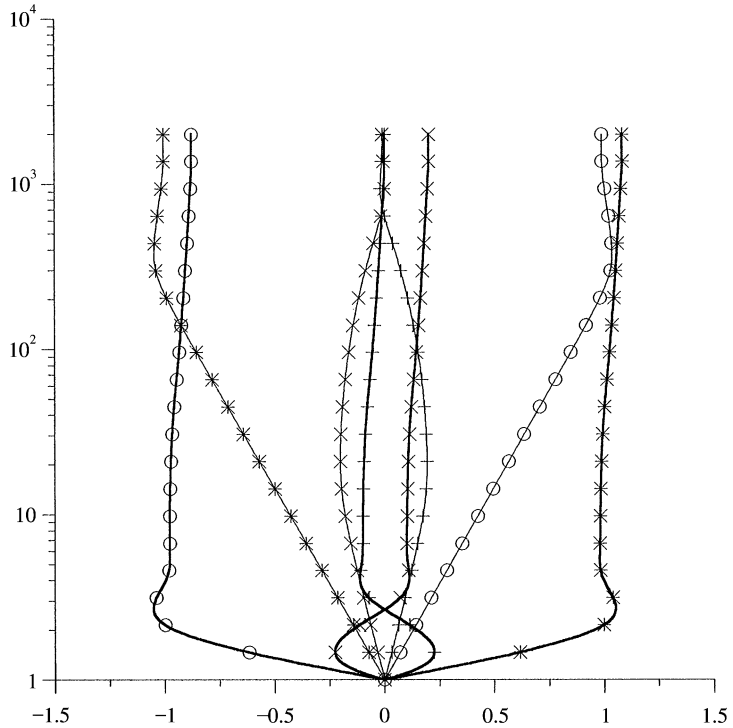

Fig. 3. Instantaneous vertical profiles of wave orbital and tidal velocities at various times of a tidal cycle. Light and heavy lines correspond to tidal and wave orbital velocities, respectively. The remaining explanations and, in particular, instants of time these profiles are referred to see Fig. 1.

(Smith, 1977)

$$U_T = \frac{U_{*T}}{\kappa}(1+\gamma)^{-1}\ln\frac{z}{z_0}, \quad z \leqslant \delta_W, \tag{1}$$

$$U_T = \frac{U_{*T}}{\kappa}\left[\ln\left(\frac{z}{z_0}+\gamma\frac{\delta_W}{z_0}\right) - \ln(1+\gamma) - \gamma(1+\gamma)^{-1}\ln\frac{\delta_W}{z_0}\right], \quad z \geqslant \delta_W, \tag{2}$$

where U_T is the tidal velocity amplitude; $\gamma = U_{*W}/U_{*T}$; U_{*W} and U_{*T} are the amplitudes of wave and tidal bottom friction velocities, respectively; δ_W is the wave BBL height defined as $\delta_W = \kappa U_{*W}/\sigma_W$; σ_W is the wave frequency; z_0 is the bottom roughness length; κ is von Karman's constant; and z is the height above the bottom.

We define the drag coefficient in a tidal flow with the presence and the absence of wind waves (c_D and c_{D0}, respectively) by the expressions

$$c_D^{-1/2} = U_{T1}/U_{*T}, \quad c_{D0}^{-1/2} = \frac{1}{\kappa}\ln\frac{z_1}{z_0}, \tag{3}$$

where z_1 is a reference height within the bottom logarithmic layer but above the wave BBL; U_{T1} is the tidal velocity at this height. Then from Eqs. (2) and (3) it follows that to first order in $\gamma\delta_W / z_1$:

$$c_D^{-1/2} = c_{D0}^{-1/2} - \frac{1}{\kappa}\left[\ln(1+\gamma) + \gamma(1+\gamma)^{-1}\ln\frac{\delta_W}{z_0} - \gamma\left(\frac{z_1}{z_0}\right)^{-1}\frac{\delta_W}{z_0}\right], \tag{4}$$

where $c_D = c_{D0}$ at $\gamma = 0$ and $c_D > c_{D0}$ at $\gamma > 0$, $[\ln(1+\gamma)(\delta_W/z_0)^{\gamma/(1+\gamma)}] > \gamma(z_1/z_0)^{-1}(\delta_W/z_0)$. That is, since wave-current interaction basically occurs in the BBL, physically this implies an enhaced drag coefficient at a reference height above the bottom. The parameters γ and δ_W/z_0 appearing in Eq. (4) are related to $U_{*W}/U_{W\infty}$, $U_{*T}/U_{T\infty}$ and $Ro_W = U_{W\infty}/\sigma_W z_0$ by the relationships

$$\gamma = \left(\frac{U_{*W}}{U_{W\infty}}\right)\left(\frac{U_{*T}}{U_{T\infty}}\right)^{-1}\left(\frac{U_{W\infty}}{U_{T\infty}}\right), \tag{5}$$

$$\frac{\delta_W}{z_0} = \kappa\frac{U_{*W}}{U_{W\infty}}Ro_W, \tag{6}$$

where Ro_W is the wave surface Rossby number; $U_{W\infty}$ and $U_{T\infty}$ are, respectively, the near-bottom wave orbital velocity amplitude and the friction-free tidal velocity amplitude. In the case when the tidal BBL extends over the whole water column and is thicker than the bottom logarithmic layer, the friction-free tidal velocity amplitude should be replaced by the surface tidal velocity amplitude.

With this reservation, the drag coefficient in a wave-affected tidal flow, c_D , is a function of the four arguments: $U_{*W}/U_{W\infty}$, $U_{*T}/U_{T\infty}$, Ro_W and $U_{W\infty}/U_{T\infty}$. The first two of them, being herein taken to mean the dimensionless wave and tidal bottom friction velocity amplitudes, are to be found; the others that involve the external parameters determining the vertical structure of the wave and tidal BBLs are considered to be prescribed.

To find $U_{*W}/U_{W\infty}$ and $U_{*T}/U_{T\infty}$, we resort to the fact that the bottom friction velocity oscillations with wave and tidal frequencies are weakly correlated and use standard boundary layer scaling arguments. In other words, we invoke the resistance law for an oscillatory turbulent BBL over a hydrodynamically rough bottom (see Appendix B), which is applicable for both the wave and tidal BBLs:

$$\ln Ro - \ln\frac{\kappa U_\infty}{U_*} + \ln\kappa^2 = [(2.3A)^2 + (2.3B + \ln 2^{-5/2}\kappa + \kappa U_\infty/U_*)^2]^{1/2}, \tag{7}$$

$$\tan\varphi_0 = 2.3A\left(2.3B + \ln 2^{-5/2}\kappa + \kappa U_\infty/U_*\right)^{-1}. \tag{8}$$

In terms of the wave factor $f_w = 2(U_*/U_\infty)$ it is rewritten as

$$\log_{10} Ro - \log_{10}\frac{1}{4\sqrt{f_W}} + \log_{10}2^{-5/2}\kappa = \left[A^2 + \left(B + \log_{10}2^{-5/2}\kappa + \frac{2^{5/2}\kappa}{2.3}\frac{1}{4\sqrt{f_W}}\right)^2\right]^{1/2}, \tag{9}$$

$$\tan\varphi_0 = A\left(B + \log_{10}2^{-5/2}\kappa + \frac{2^{5/2}\kappa}{2.3}\frac{1}{4\sqrt{f_W}}\right)^{-1}. \tag{10}$$

With $\varphi_0=0$ adopted and $(2^{5/2}\kappa/2.3)$ replaced by 1, these relationships are reduced to Jonsson's formula (Jonsson, 1966)

$$\frac{1}{4\sqrt{f_W}}+\log_{10}\frac{1}{4\sqrt{f_W}}=\log_{10} Ro-B.$$

Constants A and B appearing in Eqs. (9) and (10) are usually determined from the laboratory measurement data. In so doing the phase shift, φ_0, *is* usually taken to be zero, the assumption equivalent to specifying $A=0$ and hence to overestimating the constant B. The fact that this assumption is restrictive is easily verified. Indeed, substitution in Eqs. (9) and (10) of the values of φ_0 , f_W and Ro derived from the laboratory measurement data of Jonsson (1980) and Sumer et al. (1987) gives $A=0.92$ and $B=1.38$. Whereas, at $\varphi_0=0$ and the two other parameters being the same, we have $A=0$ and $B=1.59$. In what follows we shall apply $A=0.92$ and $B=1.38$.

Let us turn back to expression (4) and, taking into account Eqs. (6) and the relationship $\ln(\delta/z_0)=[(2,3A)^2+(2,3B+\ln 2^{-5/2}\kappa+\kappa U_\infty/U_*)^2]^{1/2}$ (see Appendix B), rewrite it in the form

$$c_D^{-1/2}=c_{D0}^{-1/2}-\frac{1}{\kappa}\left\{\ln(1+\gamma)+\gamma(1+\gamma)^{-1}\left[(2.3A)^2+\left(2.3B+\ln 2^{-5/2}\kappa+\kappa U_{W\infty}/U_{*W}\right)^2\right]^{1/2}\right.$$
$$\left.-\gamma(z_1/z_0)^{-1}\exp\left[(2.3A)^2+\left(2.3B+\ln 2^{-5/2}\kappa+\kappa U_{W\infty}/U_{*W}\right)^2\right]^{1/2}\right\}, \quad (11)$$

We next approximate Eqs. (8) and (7) by the formulae

$$U_\infty/U_*=-4.64+1.24\ln^{1.17} Ro, \quad (12)$$

$$\varphi_0(\text{deg.})=-2.74+309.2\ln^{-1.14} Ro, \quad (13)$$

which, in the range from 2×10^3 to 10^8 for Ro, is consistent with the above equations with the rms error of 0.049 for U_∞/U_* and 0.4° for φ_0. Here, as before, all the designations are given without the subscripts W and T. This implies that, as a consequence of their weak interaction, the wave and tidal bottom friction velocities may be considered as being independent of each other and described by the identical expressions with different values of the external determining parameters.

Thus, we have the set of Eqs. (11)–(13) which, along with expression (5) for the bottom friction velocity amplitude ratio, determines uniquely the drag coefficient, c_D, in a wave-affected tidal flow as a function of the three arguments: the ratio of near-bottom wave orbital velocity amplitude to friction-free tidal velocity amplitude, $U_{W\infty}/U_{T\infty}$, and the wave and tidal surface Rossby numbers, $Ro_W=U_{W\infty}/\sigma_W z_0$ and $Ro_T=U_{T\infty}/\sigma_T z_0$. Here, in addition to the known designations, σ_T is the tidal frequency. It is worth noting that the application of Eqs. (5), (11)–(13) to a tidal BBL is justified if its height is smaller than water depth. In this case , the tidal BBL height is determined from the formula $\delta/z_0=\kappa^2(\kappa U_\infty/U_*)^{-1}Ro$ using an iteration procedure in U_∞/U_*. The same formula with replacing the subscript T by W is employed to evaluate the wave BBL height. The latter is typically of several centimeters thick. Accordingly, it can extend over the whole water column only in very shallow water. This situation is beyond the scope of our paper.

If, however, the tidal BBL extends to the sea surface, the case of the tidal BBL of finite depth, Eqs. (5), (11)–(13) will continue in use with a single reserve: the last two of them are applied only for evaluating U_∞/U_* and φ_0 in the wave BBL. As regards U_∞/U_* and φ_0 in the tidal BBL of finite height, these are readily calculated from the formulae

$$U_\infty/U_* = -4.75 + 3.37\ln^{0.918}(\delta/z_0), \tag{14}$$

$$\varphi_0(\text{deg.}) = 0.974 + 141.8\ln^{-1.10}(\delta/z_0), \tag{15}$$

approximating Eqs. (B.7) and (B.8) from Appendix B in the range from 10^2 to 5×10^5 for δ/z_0 with the rms error of 0.018 for U_∞/U_* and 0.015° for φ_0. Here, $\delta\equiv\delta_T=h$, that is, the tidal BBL height, δ_T, is now considered to be known and equal to the local water depth, h. Thus , in order to determine c_D from Eqs. (11)–(13) or Eqs. (11), (14), (15) the ratio of near-bottom wave orbital velocity amplitude to friction-free tidal velocity amplitude as well as the wave and tidal surface Rossby numbers (or the normalized (by z_0) local water depth) must be known.

The formulation based on Eqs. (5), (11)–(13) or (5), (11), (14), (15) can serve as an alternative to that proposed by Grant and Madsen (1979) and may be termed the weak wave–tide interaction formulation.

There are three possibilities to verify the new formulation. These are to compare the values of c_D predicted by the new formulation with those derived from Experiments of CODE-1 and CODE-2 on the northern California continental shelf, the measurement data in the Gulf of Marsden, the north-eastern coast of England, and, as suggested by a reviewer, with the 1D BBL model predictions. The first two possibilities have been studies by Kagan and Utkin (1999). They showed that the observed and predicted values of c_D are in better agreement than a strong scatter of experimental estimates suggest. The rms error in the predicted values of c_D was at least several times smaller than wave-induced changes of c_D in themselves. Verification of the third possibility demonstrates the same results. For the fixed values of $Ro_W=1.5\times10^{-2}$, $Ro_T=1.5\times10^{-2}$ and the values of $U_{W\infty}/U_{T\infty}$ varying from 0 to 10, the rms error in predictions of c_D is 0.00156 (the linear correlation coefficient is 0.8911), whereas the modelled range of wave-induced changes of c_D amounts to (0.003, 0.067). Again, it is several times smaller than the wave-induced changes of c_D.

4. Application to Cádiz Bay

4.1. Initial information and numerical model

The region chosen for the investigation is Cádiz Bay where detailed tide gauge and bottom pressure measurements along the coast and in the interior of the basin have been made. Cádiz Bay is near latitude 36.5°N on the south-west coast of Spain. It faces west to Gulf of Cádiz and is landlocked around its south-western, southern and eastern margins by the mainland. The bay is subdivided into two basins, a shallower one (Inner Bay) and a deeper one (Outer Bay), connected together by the narrow Puntales Channel. The bay is shallow, with a maximum depth of 20 m at its seaward edge, and is characterized by dominantly semidiurnal co-oscillating tides with the amplitude of ~1 m for the M_2 constituent and ~0.4 m for the S_2 constituent. The typical waves in

Cádiz Bay are short-period wind waves with the periods below 7 s and the amplitudes of ~0.5 m in summer and ~1 m in winter, although wind waves with amplitudes of more than 1 m can occur during storm events. The longer period swell components of the wave spectrum have the periods of 12–15 s and the amplitudes of about 1.5 m. Sea-bed sediments consist mainly of coarse silt with the median grain size of 40 μm and medium sand with the median grain size of 190 μm. Quartz grains comprise 85% of all the sediments (Gutiérrez et al., 1996).

The two-dimensional (2D in the horizontal), nonlinear, finite-difference, hydrodynamic model developed by Álvarez et al. (1997) was applied to simulate the spatial distributions of tidal elevation, tidal ellipse parameters and tidal energy budget characteristics for the M_2 constituent in Cádiz Bay. A condition of no flow normal to the coast was set at the land boundaries. At the open boundary, a radiation condition written in terms of the deviations of tidal elevation and tidal velocity from their observed values was employed to ensure that, when disturbances were generated, they all propagated away from the model domain. The observed values of tidal characteristics appearing in this boundary condition were evaluated as follows: the tidal elevations along the open boundary were obtained using a linear interpolation/extrapolation of those derived from the bottom pressure observations at stations Cochinos and Bajo de Cabezuelas, while the tidal velocities were taken as being equal to the M_2 velocity derived from the measurement data at the current meter mooring location at the open boundary. The effect of flooding and drying of mud flats are not considered. Instead of this, the coastal boundaries were presented as vertical walls at the local water depth equal 1 m. The bathymetry shown in Fig. 4 was taken out of the IHM chart number 443.

For the solution to be smooth the equations of motion were supplemented with smoothing terms. The latter were defined by a horizontal eddy diffusion operator acting on tidal velocity throughout the model domain except for its boundaries. The horizontal eddy viscosity coefficient was kept to a minimum of 1 $m^2 s^{-1}$ to avoid excessively strong smoothing the solution and, at the same time, to suppress short-wavelength numerical disturbances in the fields of tidal characteristics.

The near-bottom wave orbital velocity amplitude was obtained from linear wave theory using known values of wind-wave amplitude at the sea surface, wave frequency and local water depth. In shallow regions where water depths are less than twice the wave amplitude, the latter was assumed to be depth-limited due to wave breaking and equal to half the local water depth. This condition is identical with the empirical wave-breaking criterion employed by Tang and Grimshaw (1996). The applicability of linear wave theory to shallow water was verified by Dean (1986) who, based on a comparison of measured and predicted values of near-bottom wave orbital velocity, showed that this theory provided good results for a wide range of wave amplitudes and wave steepenesses.

The bottom stress was parameterized by a quadratic resistance law with the drag coefficient taken as described previously to account for the influence of wave-tide interaction. The drag coefficient in the absence of wind waves and the bottom roughness length were specified as $c_{D0} = 0.003$ and $z_0 = 0.1$ cm, respectively. This value of c_D is in rough agreement with the prescribed value of z_0 and is based upon the reference height 1 m above the bottom. Strongly speaking, these quantities cannot remain constant over the whole region of interest where there are changes in bed types and bottom sediment grain-sizes (Heathershaw, 1981). However, as a first approximation, this assumption is likely acceptable, since even in the eastern Irish Sea where

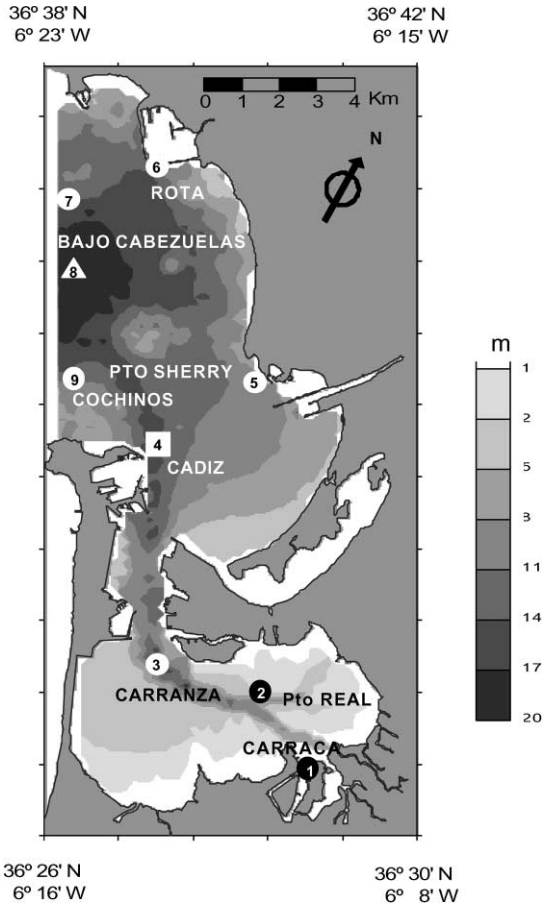

Fig. 4. Map of Cádiz Bay. Superimposed on the bathymetry, also shown are the locations of the tide gauge, bottom pressure and current meter measurements referred to in the text. The location of the tide gauge is denoted by the square, the locations of the bottom pressure sensors are denoted by open and closed circles, and the location of the current meter mooring is denoted by the triangle.

the spatial variation of bed types and forms is much more pronounced than in Cádiz Bay, no significant differences between flow fields determined with spatially varying and constant values of the drag coefficient or the bottom roughness length were found (Aldridge and Davies, 1993; Davies and Lawrence, 1995). To evaluate the tidal BBL height and hence, to decide which of the sets ((12), (13) or (15),(16)) should be used when determining $U_{T\infty}/U_{*T}$ and φ_0 in the 2D model, the formula (14) was employed with direct substitution of the depth-average tidal velocity amplitude for the friction-free tidal velocity amplitude.

We stress that in 2D integral models, the depth-averaged velocity $\mathbf{u}$, instead of the local tidal velocity, $\mathbf{u}_1$, at a fixed height, z_1, within the bottom logarithmic layer is used as a quantity specifying the bottom stress. A rough estimate of the error due to replacing $\mathbf{u}_1$ by $\mathbf{u}$ was given in Álvarez et al. (1999). It shows that bottom stresses, specified by $\mathbf{u}$ and $\mathbf{u}_1$, will differ from each

other by the factor $|\mathbf{u}|^2/|\mathbf{u}_1|^2 = \ln^2(h/2.73\ z_0)^2 \ln^{-2}(z_1/z_0)$, provided that the vertical distribution of tidal velocity in shallow waters is described by the logarithmic layer and the sense of rotation of tidal velocity remains unaltered in height within the bottom logarithmic layer. Here, as before , h is water depth. The magnitude of the above factor is greater than one at $h > 2.73\ z_1$, and smaller than one at $h < 2.73\ z_1$. Hence, the use of the depth-averaged velocity instead of the local one can give rise to an overestimation of the bottom stress at relatively great depths and its underestimation at small depths. In the case of Cadiz Bay, the bottom stress may be overestimated at $z_1 = 1\,m$ by the factor 1.5.

The tidal dynamics equations were integrated on an Arakawa C staggered grid using a semi-implicit Crank–Nicolson scheme. A spatial resolution of 210 m and a time step of 30 s were chosen. The model was run for 8 tidal cycles to achieve a stable time-periodic solution. After establishing this solution, the model run was continued for five more tidal periods, so that the amplitudes and the phases of tidal elevation and tidal velocity for the M_2 constituent could be determined by means of a harmonic analysis of the appropriate time series. Thereafter the cotidal charts and the maps of tidal ellipse parameters and mean (over a tidal cycle) tidal energy budget characteristics were constructed.

4.2. Simulation results

The simulation results for a wave amplitude of 0.5 m and a wave frequency of 5 s, along with the field of near-bottom wave orbital velocity amplitude, are presented in Figs. 5–12. Also shown here are the differences between the model predictions with and with no wave–tide interaction effects. The last case conforms to $\gamma = 0$ and hence $c_D = c_{D0}$ (see Eq. (11)).

As might be expected, the drag coefficient in the wave-affected tidal flow increases throughout Cádiz Bay (Fig. 6). The most dramatic changes up to eight-fold over the no-wave case occur in the shallow Inner Bay. These changes give rise to a marked enhancement of the mean bottom stress within the whole bay (Fig. 7). The most pronounced changes are detected in the regions of strong tidal currents, especially Puntales Channel, and in the shallows. There, the mean bottom stress is about an order of magnitude larger than that in the no-wave case. Such a significant increase in the mean bottom stress tends to decrease the tidal velocities in these regions (Fig. 8). The maximum tidal velocity is reduced by 4–8 cm s^{-1} in Puntales Channel and 2–4 cm s^{-1} in the shallows. "These findings, like those occurring in the Eastern Irish Sea (Davies and Lawrence, 1994a), are hardly surprising. In the latter, an increase in c_D by factor of over five was found due to wave–current interaction effects. It produced the decrease in bottom currents, although the resulting bottom stress field was similar to that predicted in the no-wave case".

But the fact that the wave-induced enhancement of the bottom stress is accompanied by increasing instead of decreasing the maximum tidal velocities in the deeper regions of Outer Bay is really surprising. This feature may be attributed to an amplification of the mean influx of tidal energy from Gulf of Cádiz into Cádiz Bay and its associated intensification of the mean tidal energy transport through the deeper regions of Outer Bay. Indeed, the mean tidal energy flux per unit length, $\langle \mathbf{F} \rangle$, is defined as $\langle \mathbf{F} \rangle = \langle \mathbf{u}(h+\zeta)(g\zeta + |\mathbf{u}|^2/2) \rangle$, where $\mathbf{u}$ is the depth-averaged tidal velocity vector; ζ is the tidal elevation; h is the depth; g is the acceleration due to gravity; and the angular brackets denote averaging over a tidal cycle. Let us make use of the fact that in the regions of interest the tidal elevations are much less than the local water depths, and the values of

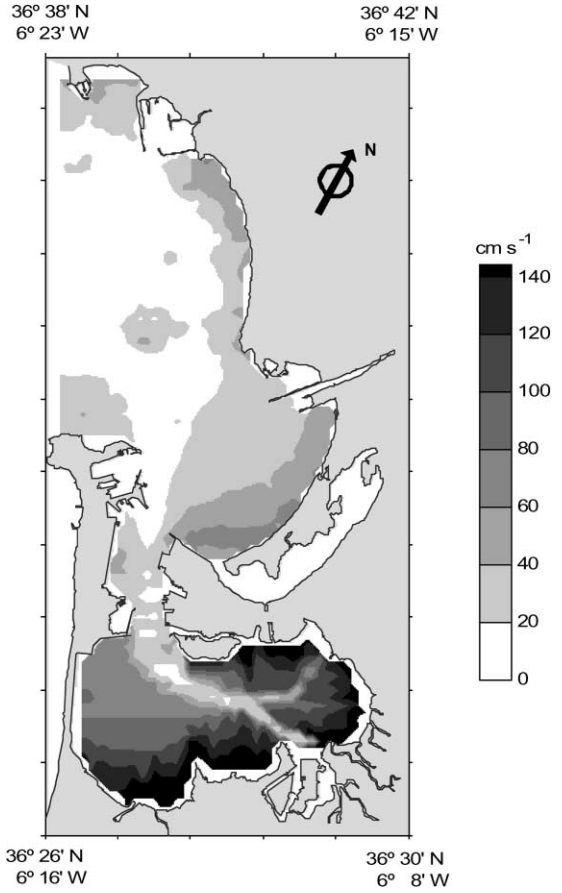

Fig. 5. Near-bottom wave orbital velocity amplitude.

the kinetic tidal energy per unit mass, $|\mathbf{u}|^2/2$, are much less than the values of the potential tidal energy per unit mass, $g\zeta$. Then, on varying the definition of $\langle \mathbf{F} \rangle$ and taking into account that the tidal currents in the above regions are nearly reversive in character (Fig. 9), we get $\delta\langle F \rangle = gh\delta\langle u\zeta \rangle$, where F is the streamwise component of $\mathbf{F}$; u is the maximum tidal velocity; and δ is the variation symbol. For time-periodic u and ζ, $\langle u\zeta \rangle = 0.5UZ\cos\phi$, where U and Z are the ampitudes of u and ζ; ϕ is the phase difference between them. Consequently, $\delta\langle F \rangle = 0.5gh[Z_0\delta(U)\cos\phi_0 + U_0\delta(Z)\cos\phi_0 - U_0Z_0\sin\phi_0\delta(\phi)]$, where the quantities with the subscript '0' refer to the no-wave case. Next, the model results presented in Figs. 7 and 10 show that in the deeper regions of Outer Bay, $\delta(Z) < 0$, $\delta(\phi) > 0$ and $\phi_0 < 90^\circ$. Thus, the positive values of $\delta\langle F \rangle$, as suggested by Fig. 9, occur only if $\delta(U) > 0$. This establishes that the amplified mean influx of tidal energy from Gulf of Cádiz which is responsible for the enhanced mean tidal energy transport through the deeper regions of Outer Bay can in fact produce the above-mentioned feature in the field of maximum tidal velocity.

On making this inference, we proceeded from the assumption that the wave–tide interaction in Cádiz Bay could give rise to an increase in the mean influx of tidal energy from Gulf of Cádiz.

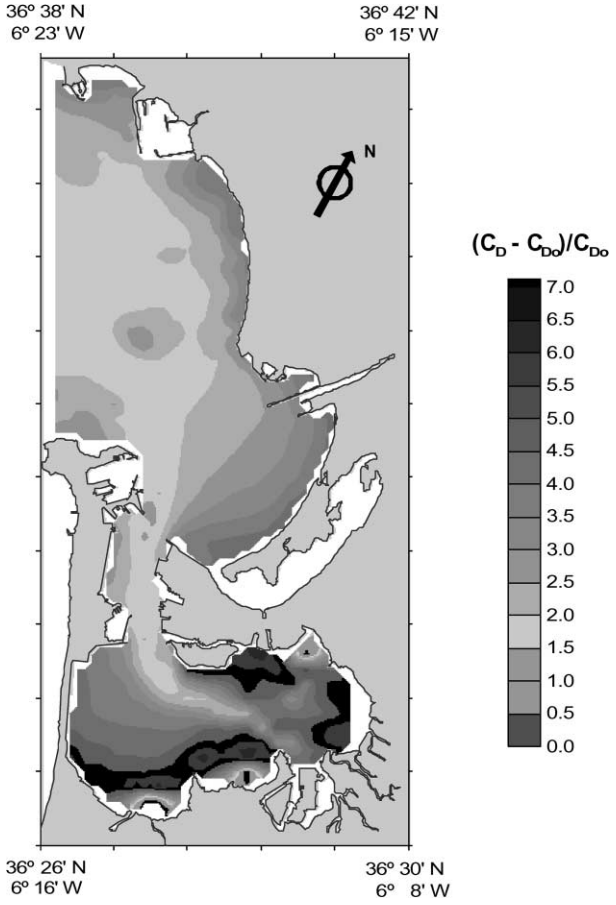

Fig. 6. Increases of the drag coefficient, in relative units, due to wave–tide interaction effects.

This assumption is supported by the model results for the mean tidal energy dissipation in Cádiz Bay (Fig. 10). As a matter of fact, in a small basin, such as Cádiz Bay, the work performed by the tide-generating force per unit time is negligible, so that the local mean tidal energy budget is only determined by the two factors: the divergence of the mean tidal energy flux per unit length and the mean tidal energy dissipation rate. Accordingly, the mean influx of tidal energy from adjacent basins is to be balanced by the integral (over the basin considered) tidal energy dissipation. Judging from Fig. 10, the latter in Cádiz Bay is enhanced under the influence of wave-tide interaction; so it is also to be for the mean influx of tidal energy from Gulf of Cádiz.

It should be remarked that the maximum changes in mean tidal energy dissipation in Cádiz Bay are confined to Puntales Channel, resulting in enhancing the mean tidal energy dissipation in this region by half over the no-wave case (Fig. 10). In the other regions of Cádiz Bay, the appropriate changes are also very significant but only in relative units: both the mean tidal energy dissipation and its changes in Outer and Inner Bays are much less than those in Puntales Channel.

We have not yet touched on how wave–tide interaction affects the fields of tidal elevation amplitude and phase. The model results for amplitudes and phases of the M_2 tidal elevations

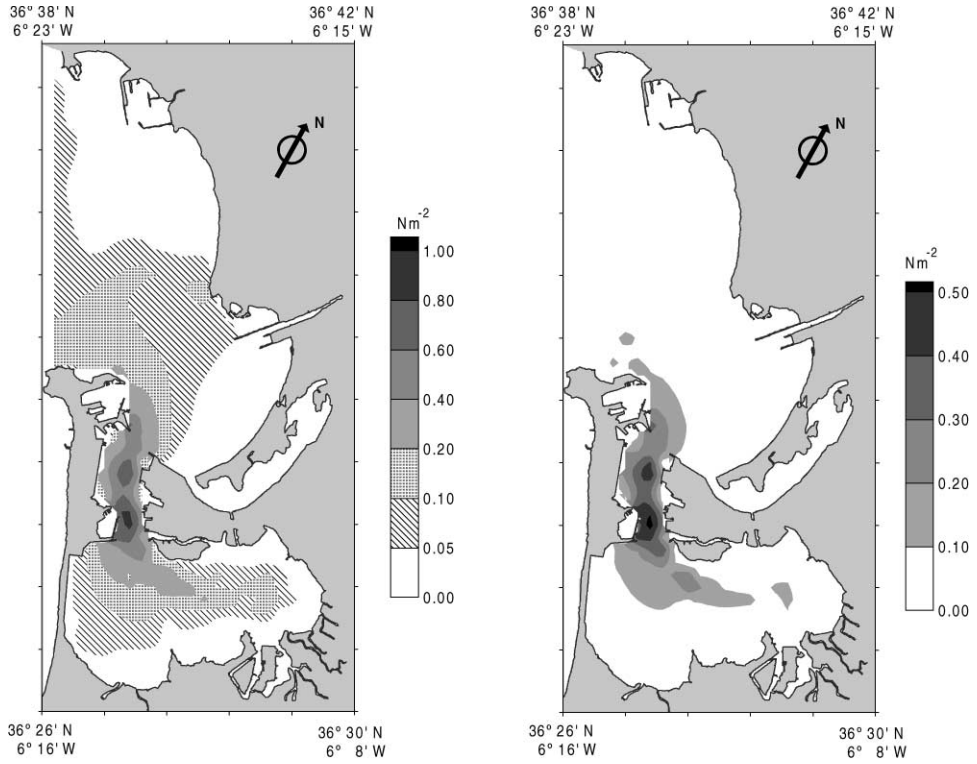

Fig. 7. Mean (over a tidal cycle) bottom stress (left) and its wave-induced changes (right).

reveal no intriguing features. As expected, the wave-enhanced bottom stress tends to decrease the tidal elevation amplitudes and to incease the tidal elevation phases throughout the bay. Their maximum changes are detected in the shallow Inner Bay, but even there these changes are of minor importance in the formation of the M_2-wave spatial structure. However no matter how small these changes are, they improve convincingly a quantitative agreement between the model predictions and the observational data at the locations of tide-gauge and bottom pressure measurements in Cádiz Bay (Table 2).

Completing the discussion of the model results obtained with and without wave–tide interaction effects, we shall dwell on one important applied aspect of the problem studied, namely identifying the domain of potential suspended sediment transport. As known, sediment particles begin to go into suspension when the bottom stress becomes equal to its critical value. The latter are determined from an empirical dependence (see, e.g., Soulsby and Wainwright, 1987) by the mean grain size of sediment particles and the ratio of the sea-bed sediment density to the sea-water density. With this information at hand, the identification of such a domain is reduced to straightforward comparison of the predicted values of maximum bottom stress (Fig. 11) and its critical value. Fig. 12 presents a plot of this domain in Cádiz Bay for the wave and no-wave cases. As is easy to see, there is a significant difference in the domain area in both the cases: if in the first case the potential suspended sediment transport domain spans Inner Bay, Puntales Channel and

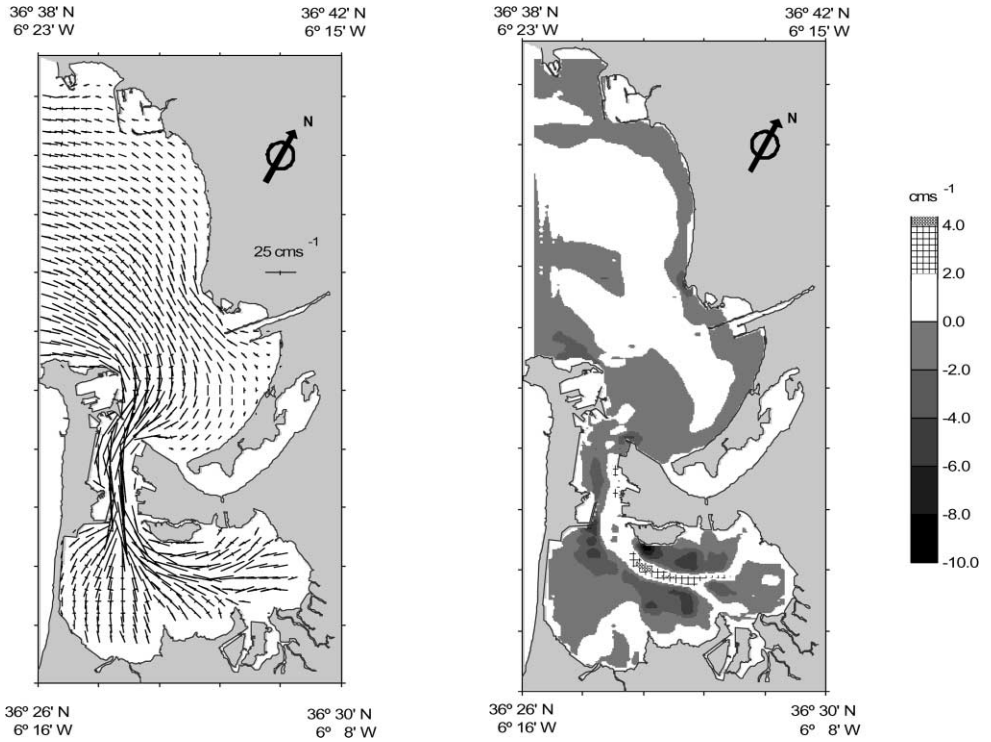

Fig. 8. Major and minor axes of tidal ellipses (left) and wave-induced changes in maximum tidal velocity (right).

the southern part of Outer Bay, then in the second case it is mainly localized within Puntales Channel and its vicinity. In quantitative terms, the area of the potential suspended sediment transport domain is increased by 30.6 km^2 (28% in relative units) over the no-wave case. This estimate, along with the estimates of the area-averaged, wave-induced changes in tidal characteristics in Inner Bay, Outer Bay and Cádiz Bay as a whole, is presented in Table 3 (see the columns labelled Exp0). The point needs to be made that the bottom stress due to wind waves is usually greater than due to tides. Therefore, it is the wind-wave bottom stress which will determine the domain of potential suspended sediment transport.

4.3. Sensitivity experiments

In the previous series of calculations which will be called Experiment 0, a wave amplitude of 0.5 m and a wave period of 5 s were set as being typical for Cádiz Bay in summer. To examine the influence of the variable wave parameters upon the tidal dynamics and energetics of Cádiz Bay and, at the same time, to gain an impression of the wave-induced seasonal variability in tidal characteristics, the following two numerical experiments were performed: in the first (Experiment 1) corresponding to typical wind waves in winter, the wave amplitude and period were taken 1.0 m and 5 s; in the second (Experiment 2) corresponding to a period of significant swell propagating into the bay from Gulf of Cádiz, these wave parameters were taken 1.5 m and 15 s, respectively.

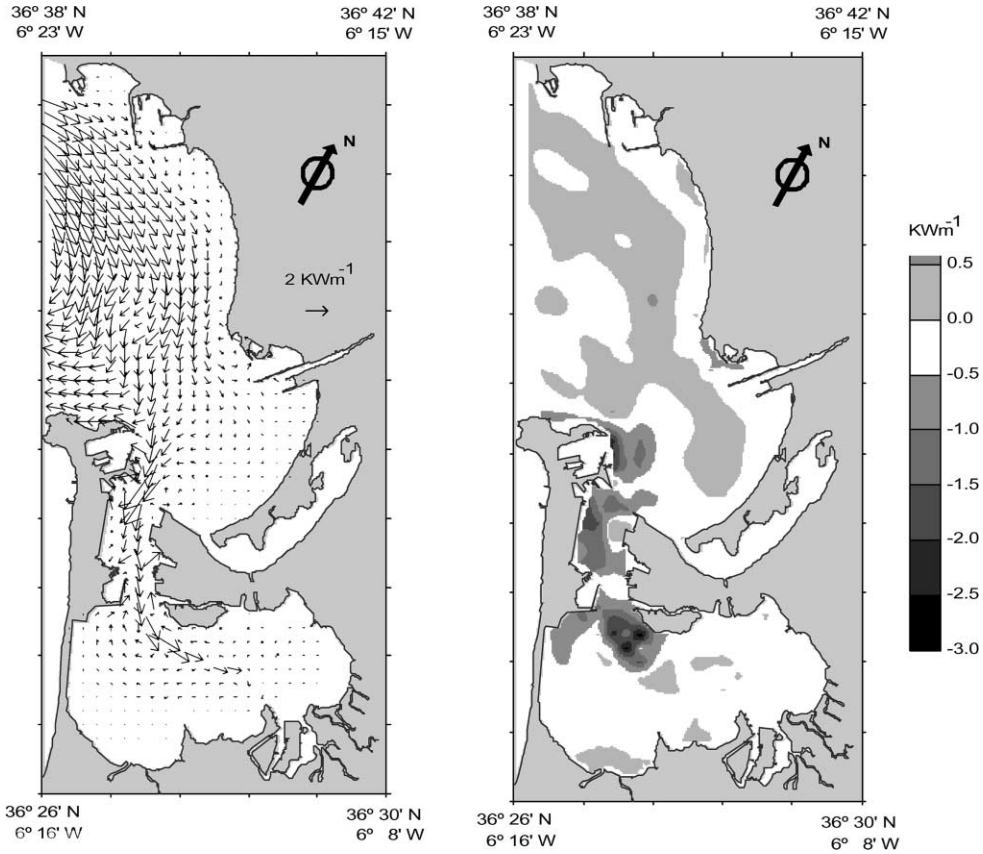

Fig. 9. Mean (over a tidal cycle) tidal energy flux per unit length (left) and its wave-induced changes (right).

The fields of the wave-induced changes in tidal characteristics obtained in both these experiments (not shown here) are qualitatively similar to those outlined in Figs. 6–12, thereby showing that in a qualitative respect the previously derived results are robust for realistic wave parameter values. As before, wave–tide interaction decreases the tidal elevation amplitude and increases the drag coefficient, tidal elevation phase and the mean tidal energy dissipation at each location in Cádiz Bay. Also, it tends to enhance the mean tidal energy fluxes at deeper depths and, on the contrary, to attenuate them in the shallows. As a result, the maximum tidal velocities still further reduce in the shallows and slightly increase at deeper depths compared to their values in Experiment 0. In a quantitative respect, the wave-induced changes in tidal characteristics increase with increasing wave amplitude and period. This is apparent from the estimates of the area-averaged changes in tidal characteristics summarized in Table 3. A point that should be particularly emphasized is that an increase in wave amplitude and period leads to spreading the domain of potential suspended sediment transport. For given values of swell amplitude and period (Experiment 2) this domain extends over the nearly whole Cádiz Bay.

Finally there is another point which merits attention. On comparing the results of Experiments 0 and 1 corresponding to the typical summer and winter wave conditions in Cádiz Bay, we see that

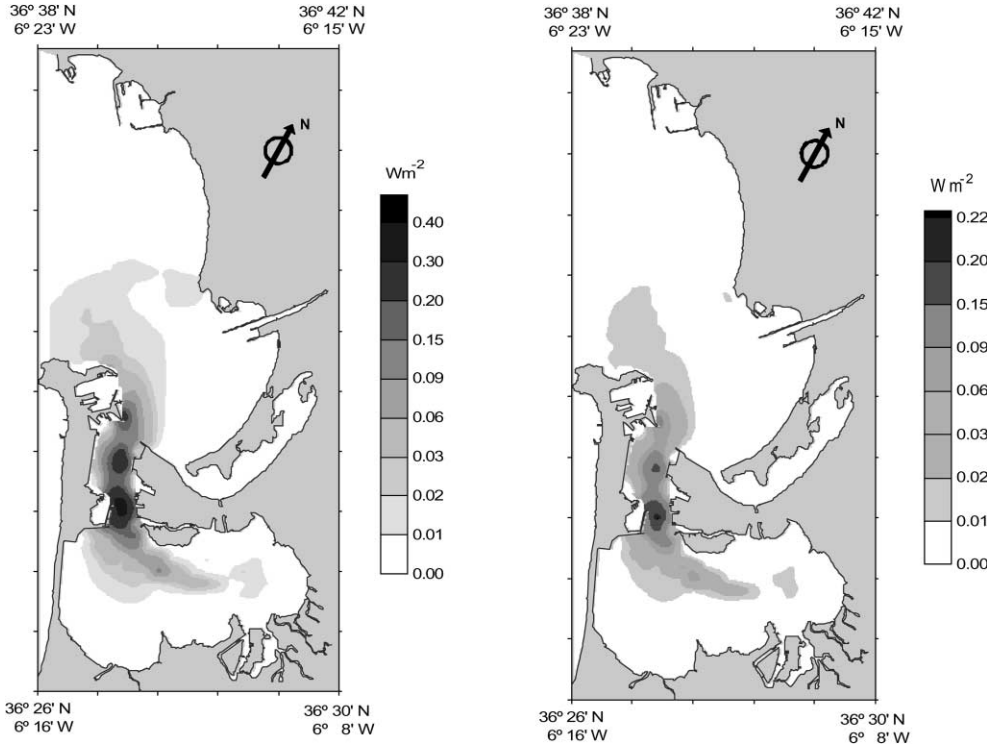

Fig. 10. Mean (over a tidal cycle) tidal energy dissipation (left) and its wave-induced changes (right).

the mere changes in tidal characteristics differ in magnitude fairly slightly and, what is more important, these changes are small compared to the values of tidal characteristics as such. This implies that the wave-induced seasonal variability in the M_2 tidal constants in Cádiz Bay may be recognized as negligible. The same is not necessarily valid for other tidal constituents (say, for the long-period ones) and/or other shallow basins, as supported by the results of Experiment 2.

It may be interesting to see if the other tidal constituents in shallow waters are enhanced by the wave–tide interaction effects. We are going to discuss this point in another paper.

5. Conclusions

In this paper we have examined the character of wave/low-frequency current interaction using, as the basis, a single-point, one-equation (k–l) model for an oscillatory turbulent BBL over a hydrodynamically rough surface. The solution of the model equations for a combined wave/low-frequency flow, accounting for the nonlinear interaction between wave and low-frequency components of motion, has been compared with the appropriate solution obtained by employing a linear superposition of the particular solutions for purely wave and low-frequency motions and hence by disregarding nonlinear interaction effects. As a result, it has been shown that a quantitative agreement between both the solutions is better, the greater are the ratio of

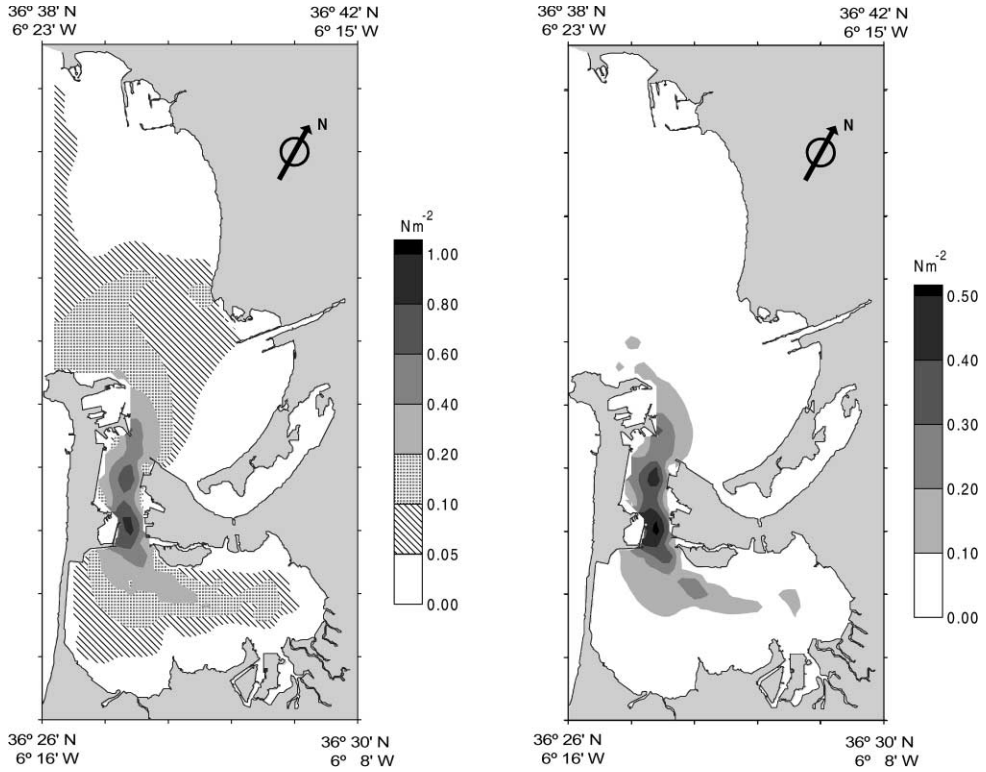

Fig. 11. Maximum value bottom stress (left) and its wave-induced changes (right).

near-bottom wave orbital velocity amplitude to friction-free, low-frequency velocity amplitude and the ratio between frequencies of wave and low-frequency components of motion. So, in the case of wave–tide interaction when the velocity amplitude ratio is of the order 1, and the frequency ratio is of the order 10^4, that is, under conditions typical of shallow waters, the linear superposition of the particular solutions for purely wave and low-frequency motions provides a high accuracy in evaluating the bottom stress: the relative mean error and the correlation between the bottom stress values calculated with and with no allowance for nonlinear interaction effects are 0.11% and 0.9992, respectively. Moreover, the vertical velocity profiles simulated at various times of a tidal cycle in both these cases are not too distinctive among themselves. This suggests that wave–tide interaction may be recognized as weak, and the bottom stress oscillations with wave and tidal frequencies as weakly correlated.

Based on this finding and the usual physical notion of continuity of the vertical eddy viscosity and the velocity at the top of the wave BBL, we have got a relationship between the drag coefficient in a wave-affected tidal flow and its determining parameters: the scaled wave friction velocity amplitude, the scaled tidal friction velocity amplitude and the ratio of near-bottom wave orbital velocity amplitude to friction-free tidal velocity amplitude. This relationship, along with the surface Rossby number dependences for the scaled wave and tidal friction velocity amplitudes that follow from the resistance law for an oscillatory turbulent BBL over a hydrodynamically

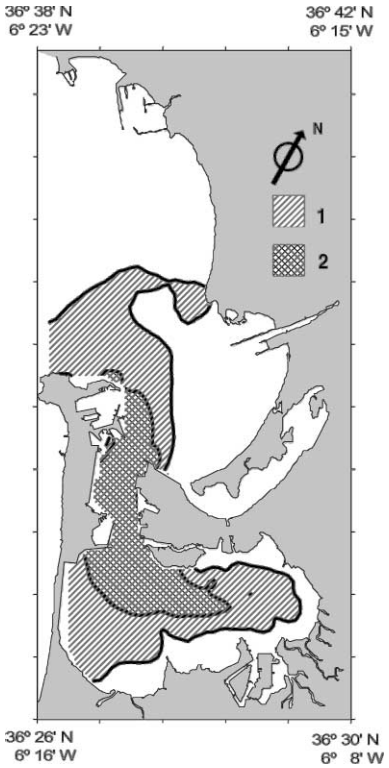

Fig. 12. Domain of potential suspended sediment transport as predicted with (1) and with no (2) wave–tide interaction effects.

Table 2
Tidal constants (The M_2 constituent) at the locations of tide gauge and bottom pressure measurements, as derived from observational evidence and the model predictions with (*a*) and with no (*b*) wave–tide interaction effects

Station	Amplitude (cm)			Phase (°)		
	Observed	Predicted		Observed	Predicted	
		a	b		a	B
CARRACA (1)	108.0	108.3	108.7	60.0	59.4	55.9
PTO. REAL (2)	106.5	108.4	108.8	57.9	59.5	56.0
P. CARRANZA (3)	107.2	107.0	107.3	57.7	57.4	54.9
PTO. CÁDIZ (4)	103.1	104.4	104.6	55.0	55.6	53.1
PTO. SHERRY (5)	103.2	103.9	104.1	52.6	54.4	53.4
ROTA (6)	101.4	103.2	103.4	53.8	54.3	53.3

rough surface, represents a formulation for weak wave–tide interaction. It can serve as an alternative to the commonly accepted formulation of Grant and Madsen (1979). A verification of the new formulation against observational evidence obtained during experiments CODE-1 and CODE-2 on the northern California Continental Shelf, the measurement data in the Marsden

Table 3
Area-averaged changes in tidal characteristics due to wave–tide interaction effects for various values of wave amplitude and period

Characteristic	Inner Bay			Outer Bay			Cádiz Bay		
	Exp 0	Exp 1	Exp 2	Exp 0	Exp 1	Exp 2	Exp 0	Exp 1	Exp 2
Drag coefficient	0.011	0.015	0.041	0.007	0.010	0.033	0.008	0.011	0.036
Amplitude of tidal elevation (cm)	−0.45	−0.71	−3.58	−0.28	−0.39	−1.33	−0.33	−0.49	−1.99
Phase of tidal elevation (°)	2.15	3.05	9.13	0.10	0.12	0.33	0.72	0.98	2.89
Maximum tidal velocity ($cm\,s^{-1}$)	−0.76	−0.99	−1.43	−0.13	−0.23	−0.52	−0.33	−0.45	−0.79
Phase difference between maximum tidal velocity and tidal elevation (°)	−5.9	−7.1	−9.9	0.1	1.1	9.1	−1.7	−1.3	3.5
Mean bottom stress ($N\,m^{-2}$)	0.06	0.14	0.40	0.06	0.06	0.19	0.06	0.08	0.26
Maximum bottom stress ($N\,m^{-2}$)	0.13	0.29	0.80	0.12	0.12	0.37	0.12	0.17	0.50
Mean tidal energy flux per unit length ($Kw\,m^{-1}$)	−0.15	−0.37	−0.41	−0.18	−0.10	−0.03	−0.17	−0.18	−0.14
Mean tidal energy dissipation ($W\,m^{-2}$)	0.01	0.03	0.08	0.01	0.01	0.02	0.01	0.01	0.04
Area of the potential suspended sediment transport domain (Km^2)	14.5	14.9	17.0	16.1	24.0	52.2	30.6	38.9	69.2

Bay, the north-eastern coast of England, and against the 1D model predictions has showed that these are in better agreement than a strong scatter of experimental estimates suggests. In all considered cases, the rms error in predictions is much less than the observed or modeled range of the wave-induced variability in c_D.

The proposed formulation has been implemented within a 2D nonlinear, finite-difference, high-resolution, hydrodynamic model, and the modified model has been applied to quantify the wave-induced changes in the M_2 tidal dynamics and energetics of Cádiz Bay. The model results obatined under typical summer wave conditions testify that, as expected, wave–tide interaction tends to increase the drag coefficient, tidal elevation phase, mean bottom stress and the mean tidal energy dissipation, on the one hand, and to decrease the tidal elevation amplitude, on the other, at each location in Cádiz Bay. At the same time, the model results reveal one unexpected feature in the fields of maximum tidal velocity and mean tidal energy flux per unit length: it turns out that wave–tide interaction is accompanied with increasing these characteristics at deeper depths and their decreasing at shallower depths. This feature, as has been clarified, is due to an overall amplification of the mean tidal energy transport into the bay from Gulf of Cádiz.

The numerical experiments on the sensitivity to varying wave parameters show that all the above features of change in the M_2 tidal characteristics are robust in a qualitative sense. The same is true for the wave-induced areal changes in the potential suspended sediment transport domain. The latter has been found to increase over the no-wave case. Overall, the wave-induced changes in M_2 tidal characteristics are small for the amplitudes and the phases of tidal elevation and tidal velocity but not for the bottom stress and tidal energy budget characteristics. These quantities per se and their changes are of the same order of magnitude. Particularly sensitive to varying wave parameters is the potential suspended sediment transport domain. If under typical summer and winter wave conditions this domain spans Inner Bay, Puntales Channel and the southern part of Outer Bay, then under conditions of significant swell it extends over the nearly whole Cádiz Bay.

With respect to magnitude the wave-induced changes in tidal characteristics in summer are not too different from those in winter. Consequently, the wave-induced seasonal variability in tidal characteristics is not pronounced in Cádiz Bay: according to our estimates, this variability for the M_2 constituent amounts to a maximum of 0.7 cm for the amplitude and 3° for the phase of tidal elevation, being small compared to the mere values of the tidal constants. However the possibility of the wave-induced seasonal variability in tidal constants being well defined in other shallow basins and/or in other tidal frequency bands must not be ruled out.

Our formulation for wave–tide interaction, like any one of formulations, is not free of shortcomings. These are mainly associated with the assumptions that (i) rotation effects are small, so that the resistance law for a one-dimensional (in a horizontal plane) wave-affected tidal flow may be applied; (ii) waves and M_2 tidal currents are colinear; (iii) the whole random wave field may be represented by only one wave component; (iv) a wave amplitude is constant throughout the bay except for the very shallow near-coastal regions where it is specified by an empirical wave-breaking criterion; (v) the wave-breaking criterion is set at a constant value, no matter what it is a function of location and hence local depth; (vi) even in the case of breaking waves, linear wave theory is used to evaluate the near-bottom wave orbital velocity amplitude.

The majority of these assumptions are reasonable for Cádiz Bay where, because of the absence of significant variations of depth, the tidal currents are inherently reversive in character, and the waves propagate from the open boundary to the surf-zone without appreciable reflection or backscattering. However it is difficult if not impossible to imagine that such a situation occurs in other shallow basins. That is why the proposed formulation needs improvement in many respects. This is first of all concerned with the resistance law which should be generalized to the case of a two-dimensional (in a horizontal plane) tidal BBL over a hydrodynamically rough bottom. In this case, the only determining parameter (the surface Rossby number or the ratio of water depth to bottom roughness length depending on, respectively, whether we are dealing with an asymptotic BBL or a BBL of finite depth) has to be supplemented by three more determining parameters. These are the ratio between inertial and tidal frequencies, the ratio between amplitudes of friction-free tidal velocity vector components, and the phase difference between them (Kagan, 1972). It would be of interest to clear up, whenever possible, how the resistance law is modified in this four-dimensional parameter space.

Another aspect of the formulation which calls for improvement is related to invoking a proper procedure for determining single wave parameters or, as has been suggested by Davies and Lawrence (1995), a wind-wave spectrum so as to transform it to a characteristic near-bottom wave orbital velocity amplitude. In the last case, it should be borne in mind, among other things, that at

each location there are both breaking and unbroken waves and that, hence, the concept of a wave-breaking criterion or a maximum possible wave amplitude at a given water depth is to be revised. It is also desirable to give up the assumption of colinearity of waves and tidal currents, since, as has been established by Grant and Madsen (1979), this assumption is adequate only if the angle between waves and currents is less than 60° or a near-bottom wave orbital velocity amplitude is much greater than a friction-free tidal velocity amplitude. Thus, a great deal needs to be done before wave-tide interaction and its consequences become well understood.

Acknowledgements

The work was carried out during a stay of B. A. Kagan as visiting professor at University of Cádiz and was partially supported by the INTAS Programme in the framework of the Project 96-1875 and NATO Linkage Grant no. EST.CLG 975279. The authors would like to thank the anonymous reviewers for valuable remarks.

Appendix A

A.1. A single-point, one-equation, turbulence (k–l) model

The model in use a single-point, one equation, turbulence (k–l) model in which the sought for variables are the velocity, vertical eddy viscosity, turbulent-kinetic energy (TKE), TKE dissipation rate and the mixing length. Let us consider the case when the turbulent BBL extends over the whole water column and, following Charney (1969), assume that the effective vertical eddy viscosity in the BBL is limited from above by the estimate $k_e \geqslant Uh\,Re_c^{-1}$, where U is the velocity amplitude in a friction-free flow; h is the water depth (or the BBL height if it is smaller than the water depth) and $Re_c \approx 160$ is the critical Reynolds number for the oscillatory, turbulent BBL. Let us define the characteristic scales for the velocity, vertical eddy viscosity, mixing length, TKE, length and time as U, $Uh\,Re_c^{-1}$, $c_\mu^{1/4} h\,Re_c^{-1/2}$, $c_\mu^{-1/2} U^2\,Re_c^{-1}$, h and σ^{-1}, respectively. Here, σ is the prescribed tidal frequency and, $c_\mu = 0.125$ is the numerical constant in the Kolmogorov similarity relationship for the TKE dissipation rate. Then the equations for the above variables in the dimensionless form are written as

$$Sh\frac{\partial}{\partial t_n}(u_n - u_{fn}) = \frac{\partial}{\partial z_n}\left(Re_0^{-1} + Re_c^{-1}\,k_n\right)\frac{\partial u_n}{\partial z_n}, \tag{A.1}$$

$$c_\mu^{-1/2} Sh\frac{\partial b_n}{\partial t_n} = c_\mu^{-1/2}\frac{\partial}{\partial z_n}\left(\alpha_M^{-1}\,Re_0^{-1} + \alpha_{bT}^{-1}\,Re_c^{-1} k_n\right)\frac{\partial b_n}{\partial z_n} + k_n\left|\frac{\partial u_n}{\partial z_n}\right|^2 - \frac{b_n^2}{k_n}, \tag{A.2}$$

$$k_n = l_n\sqrt{b_n}, \tag{A.3}$$

$$l_n = \kappa\,\mathrm{Re}_c^{1/2}(b_n/b_{on})^{1/2}\left(z_n + \int_{Z_{on}}^{Z_n}(b_n/b_{on})^{-1/2}\,\mathrm{d}z_n\right), \tag{A.4}$$

where $Sh=\sigma h/U$ is the Strouhal number; $Re_0=Uh/v$ is the flow Richardson number based upon the molecular viscosity v; $\alpha_M=12.5$ is the molecular Schmidt number; $\alpha_{bT}=1.37$ is the turbulent Prandtl number; u_n and u_{fn} are the dimensionless velocity and its value in the friction-free flow; k_n is the dimensionless vertical eddy viscosity; l_n is the dimensionless mixing length; b_n and $b_{on}=(Re_o^{-1}+Re_c^{-1}k_n)\ |\partial u_n/\partial z_n|z_n=z_{on}$ are the dimensionless TKE and its value at the roughness length z_{on}; κ is von Karman's constant; z_n is the dimensionless vertical coordinate directed upwards; and t_n is dimensionless time.

Eqs. (A.1)–(A.4) describe, respectively, the momentum budget, the TKE budget, the Kolmogorov similarity relationship for the vertical eddy viscosity and the integral analogue of generalized von Karman's formula for the mixing length.

A no-slip condition

$$u_n = 0, \tag{A.5}$$

and a zero vertical TKE flux condition

$$\left(\alpha_M^{-1} Re_0^{-1} + \alpha_{bT}^{-1} Re_c^{-1} k_n\right)\frac{\partial b_n}{\partial z_n} = 0, \tag{A.6}$$

are set at a bottom roughens length (at $z_n=z_{on}$). At the sea surface (at $z_n=1$), zero vertical flux of momentum and TKE are prescribed:

$$(Re_0^{-1} + Re_c^{-1}\, k_n)\frac{\partial u_n}{\partial z_n} = 0, \tag{A.7}$$

$$\left(\alpha_M^{-1}\ Re_0^{-1} + \alpha_{bT}^{-1}\ Re_c^{-1}\, k_n\right)\frac{\partial b_n}{\partial z_n} = 0. \tag{A.8}$$

If the BBL extends over the whole water column, these boundary conditions may be replaced by the asymptotic ones $u_n \to u_{fn}$; $b_n \to 0$ at $z_n \to \infty$ whereby the TKE is assumed to tend to zero, and the velocity to tend to its friction-free value as the height above the bottom increases. Notice that in the absence of wind, density stratification and wave breaking, u_{fn} remains constant in height.

Instead of initial conditions, the time-periodic conditions for velocity and TKE

$$u_n(t_n) = u_n(t_n + 2\pi);\ b_n(t_n) = b_n(t_n + 2\pi) \tag{A.9}$$

are employed. If one is not interested in a transient period, these conditions are not contradictory to those used by Davies and Lawrence (1995). According to their procedure, model equations are integrated forward in time from a state of rest with M_2 — tidal forcing at open boundaries and after establishing of a time-periodic regime, the sought for variables are harmonically analyzed yielding the required amplitudes and phases.

These equations and boundary conditions, being first rewritten in terms of the deviations of velocity from its friction-free value, are solved at a given change in the friction-free velocity in time. In so doing, the water depth is specified such that the tidal velocity in the upper layer reaches its friction-free value, the linear vertical coordinate is transformed into the logarithmic one by the relationship $\xi=\ln(z_n/z_{0n})$ and the friction-free velocity is represented as the sum of two harmonic oscillations with different amplitudes and frequencies

Eqs. (A.1)–(A.9) are integrated using a semi-implicit finite-difference scheme with central differencing in the vertical and one-side differencing in time. A time step which is limited from above by the condition for high-frequency wave orbital oscillations to be resolved is taken as (2π/30) times the ratio between frequencies of low-frequency and wave components of motion. The amount of levels in the transformed vertical is taken as 200.This amount of levels is more than sufficient to resolve the near-bottom region of maximum velocity shear in the wave BBL and its overlying logarithmic layer produced by a specified low-frequency flow.

Appendix B

B.1. The resistance law for an oscillatory turbulent BBL over a hydrodynamically rough surface

Let us define the wave orbital velocity or the tidal velocity within and outside the appropriate BBL as $u = Re\, U \exp[\mathrm{i}(\sigma t + \varphi)]$ and $u_\infty = Re\, U_\infty \exp(\mathrm{i}\sigma t)$, respectively. Here, U and U_∞ are the velocity amplitudes in the BBL and the friction-free flow; σ is the oscillation frequency; and φ is the phase shift between u and u_∞. Accordingly, the expression for the velocity defect, $(u-u_\infty) = Re(U-U_\infty) \exp[\mathrm{i}(\sigma t-\pi-\varphi_d)]$, where $(U-U_\infty)$ and φ_d are, respectively, the velocity defect amplitude and the phase shift between $(u-u_\infty)$ and u_∞, which can be expressed in terms of U, U_∞ and φ as

$$(U - U_\infty) = [U^2 \sin^2\varphi + (U_\infty - U\cos\varphi)^2]^{1/2},\ \tan\varphi_d = U/(U_\infty - U\sin\varphi).$$

Similarly, we define the bottom friction velocity amplitude in the wave or tidal BBL as $U_* = (|\tau_b|/\rho)^{1/2}$ and, following Jonsson (1980), take U_* as a characteristic velocity scale in this BBL. Here,τ_b is the bottom stress; and ρ is the mean density of sea water.

Then the vertical distribution of the dimensionless (normalized by U_*) velocity in the region of small heights above a hydrodynamically rough surface will be described by the expression

$$\frac{u}{U_*} = Re\, f_u\left(\frac{z}{z_o}\right)\exp[\mathrm{i}(\sigma t + \varphi_0)], \tag{B.1}$$

where $f_u(z/z_o)$ is a non-negative function of its arguments; and φ_o is a phase shift between near-bottom and friction –free velocities, the shift which remains constant within the near-bottom layer and must be found.

Evidence from laboratory and field measurements (Jonsson, 1980; Marchuk and Kagan, 1977) as well as results of direct simulation of an oscillatory turbulent BBL over a hydrodynamically rough surface (Spalart and Baldwin, 1989) indicate convincingly that the vertical distribution of velocity adheres to the law of the wall (Eq. (B.1) with $f_u(z/z_o) = (1/\kappa)\ln(z/z_0)$ in the near-bottom layer and the velocity defect law

$$\frac{u - u_\infty}{U_*} = Re\frac{1}{\kappa}\psi_u\left(\frac{z}{\delta}\right)\exp[\mathrm{i}(\sigma t - \pi - \varphi_d)], \tag{B.2}$$

in the outer part of the BBL. Here, $\psi_u(z/\delta)$ is a non-negative, decreasing function of its argument; and δ is the height of the oscillatory turbulent BBL.

At the intermediate heights (in the region of overlapping), the asymptotic expansions (B.1) and (B.2) have to be matched. On equating the real and imaginary parts of these expressions, we come to the relationships

$$\ln\left(\frac{\delta}{z_o}\right)\cos\varphi_o - \frac{\kappa U_\infty}{U_*} = -\ln\left(\frac{z}{\delta}\right)\cos\varphi_o - \psi_u\left(\frac{z}{\delta}\right)\cos\varphi_d, \tag{B.3}$$

$$\ln\left(\frac{\delta}{z_o}\right)\sin\varphi_o = -\ln\left(\frac{z}{\delta}\right)\sin\varphi_o + \psi_u\left(\frac{z}{\delta}\right)\sin\varphi_d. \tag{B.4}$$

The left-hand side of relationships (B.3) and (B.4) is independent of z and the same is to be for the right-hand sides. Let

$$\lim_{z/\delta\to 0}\left[-\ln\left(\frac{z}{\delta}\right)\sin\varphi_o + \psi_u\left(\frac{z}{\delta}\right)\sin\varphi_d\right] = 2.3A, \tag{B.5}$$

$$\lim_{z/\delta\to 0}\left[-\ln\left(\frac{z}{\delta}\right)\cos\varphi_o - \psi_u\left(\frac{z}{\delta}\right)\cos\varphi_d\right] = 2.3B + \ln 2^{-5/2}\kappa, \tag{B.6}$$

where the factor $\ln 10 \approx 2.3$ before the numerical constants A and B as well as the second term on the right-hand side of equality (B.5) are introduced for the sake of convenience. Then, on rearrangement, we obtain

$$\ln\left(\frac{\delta}{z_o}\right) = \left[(2.3A)^2 + \left(2.3B + \ln 2^{-5/2}\kappa + \kappa U_\infty/U_*\right)^2\right]^{1/2}, \tag{B.7}$$

$$\tan\varphi_o = 2.3A\left(2.3\,B + 2^{-5/2}\kappa + \kappa U_{\infty/U_*}\right)^{-1}, \tag{B.8}$$

where, with allowance made for the equality $\delta/z_0 = \kappa^2(\kappa U_\infty/U_*)^{-1}Ro$ following immediately from the definition $\delta = \kappa U_*/\sigma$, we find

$$\ln Ro - \ln\frac{\kappa U_\infty}{U_*} + \ln\kappa^2 = \left[(2.3A)^2 + \left(2.3B + \ln 2^{-5/2}\kappa + \frac{\kappa U_\infty}{U_*}\right)^2\right]^{1/2}, \tag{B.9}$$

Relationships (B.8) and (B.9) represent the resistance law for an oscillatory turbulent BBL over a hydrodynamically rough surface.

References

Aldridge, J.N., Davies, A.M., 1993. A high resolution three-dimensional hydrodynamic tidal model of the eastern Irish Sea. Journal of Physical Oceanography 23, 207–224.

Álvarez, O., Izquierdo, A., Tejedor, B., Mañanes, R., Tejedor, L., Kagan, B.A., 1999. The influence of sediment load on tidal dynamics, a case study: Cádiz Bay. Estuarine, Coastal and Shelf Sciences 48, 439–450.

Álvarez, O., Tejedor, B., Tejedor, L., 1997. Simulación hidrodinámica en el área de la Bahía de Cádiz. Análisis de las constituyentes principales. In: IV Jornadas Españolas de Ingeniería de Puertos y Costas. Servicio de Publicaciones de la Universidad Politécnica de Valencia-98, Vol. 2125, pp. 125–136.

Bender, L.C., Wang, K.-C., 1993. The effect of wave-current interaction on tidally forced estuarine circulation. Journal of Geophysical Research 98, 16,521–16,528.

Charney, G.,1969. What determines the thickness of the planetary boundary layer in a neutrally stratified atmosphere? Oceanologiya 9, 143–145.

Christoffersen, J.B., Jonsson, I.G., 1985. Bed friction and dissipation in a combined current and wave motion. Ocean Engineering 12, 387–423.

Davies, A.M., Glorioso, P.D., 1999. Near-shore wave-current interaction processes, their effects upon wind driven currents and pollutant transports. In: Moore, C. (Ed.), Coastal Ocean Predictions, Vol. 56. AGU Series, Washington, DC.

Davies, A.M., Jones, J.E., 1991. On the numerical solution of the turbulent energy equations for waves and tidal flow. International Journal of Numerical Methods in Fluids 12, 17–41.

Davies, A.M., Lawrence, J., 1994a. Examining the influence of wind and wind-wave turbulence on tidal currents, using a three-dimensional hydrodynamic model including wave-current interaction. Journal of Physical Oceanography 24, 2441–2460.

Davies, A.M., Lawrence, J., 1994b. Modelling the non-linear interaction of wind and tide: its influence on current profiles. International Journal of Numerical Methods in Fluids 18, 163–188.

Davies, A.M., Lawrence, J., 1995. Modelling the effect of wave-current interaction on the three-dimensional wind driven circulation of the eastern Irish Sea. Journal of Physical Oceanography 25, 29–45.

Davies, A.M., Soulsby, R.L., King, H.L., 1988. A numerical model of the combined wave and current bottom boundary layer. Journal of Geophysical Research 93, 491–508.

Dean, R.G., 1986. Intercomparison of near-bottom kinematics by several wave theories and field and laboratory data. Coastal Engineering 9, 399–437.

Grant, W.D., Madsen, O.S., 1979. Combined wave and current interaction with a rough bottom. Journal of Geophysical Research 84, 1797–1808.

Green, M.O., Rees, J.M., King, H.L., 1990. Evidence for the influence of wave-current interaction in a tidal boundary layer. Journal of Geophysical Research 95, 9629–9644.

Gutiérrez, J.M., Achab, M., Parrado, J.M., 1996. Distribution of recent facies at the bottom of the Bay of Cádiz. Geogaceta 21, 155–157.

Heathershaw, A.D., 1979. The turbulent structure of the bottom boundary layer in a tidal current. Geophysical Journal of the Royal Astronomical Society 58, 395–430.

Heathershaw, A.D., 1981. Comparison of measured and predicted sediment transport rates in tidal currents. Marine Geology 42, 75–104.

Johns, B., 1975. The form of the velocity profile in a turbulent shear wave boundary layer. Journal of Geophysical Research 80, 5109–5112.

Johns, B., 1978. The modelling of tidal flow in a channel using a turbulence energy closure scheme. Journal of Physical Oceanography 8, 1042–1049.

Johns, B., Oguz, T., 1987. Turbulent energy closure schemes. In: Heaps, N.S. (Ed.), Three-Dimensional Coastal Ocean Models. American Geophysical Union, Washington, DC, pp. 17–40.

Jonsson, I.G., 1966. Wave boundary layers and friction factors. Proceedings of the 10th Coastal Engineering Conference, pp. 127–148.

Jonsson, I.G., 1980. A new approach to oscillatory rough turbulent boundary layers. Ocean Engineering 46, 75–123.

Kagan, B.A., 1972. On the resistance law in tidal flow. Izvestiya. Atmospheric and Oceanic Physics 8, 533–542.

Kagan, B.A., Utkin, K.B., 1999. Weak wave-tide interaction and the drag coefficient in a tidal flow. Izvestiya, Atmospheric and Oceanic Physics, accepted.

Keen, T.R., Glenn, S.M., 1995. A coupled hydrodynamic-bottom boundary layer model of storm and tidal flows in the Middle Atlantic Bight of North America. Journal of Physical Oceanography 25, 391–406.

Kemp, P.H., Simons, B.R., 1982. The interaction between waves and a turbulent current: waves propagating with the current. Journal of Fluid Mechanics 116, 227–250.

Lou, J., Ridd, P.V., 1997. Modelling of suspended sediment transport in coastal areas under waves and currents. Estuarine, Coastal and Shelf Science 45, 1–16.

Marchuk, G.I., Kagan, B.A., 1977. Ocean Tides. Gidrometeoizdat, Leningrad, 295 pp. (in Russian), Pergamon Press, Oxford 1984 (in English).

Signell, R.P., Beardsley, R.C., Graber, H.C., Capotondi, A., 1990. Effect of wave-current interaction on wind-driven circulation in narrow, shallow embayments. Journal of Geophysical Research 95, 9671–9678.

Smith, J.D., 1977. Modelling sediment transport on continental shelves. In: Goldberg, E.D., McCave, I.N., O'Brien, J.J., Steele, J.M. (Eds.), The Sea, vol. 6. Wiley-Interscience, New York, pp. 539–577.

Soulsby, R.L., Wainwright, B.L.S.A., 1987. A criterion for the effect of suspended sediment on near-bottom velocity profiles. Journal of Hydraulic Research 25, 341–355.

Spalart, P.P., Baldwin, B.S., 1989. Direct simulation of a turbulent oscillating boundary layer. In: Andre, J.C. (Ed.), Turbulent Shear Flows, vol. 6. Springer-Verlag, Berlin, pp. 417–440.

Spaulding, M.L., Isaji, T., 1987. Three-dimensional continental shelf hydrodynamic model including wave-current interaction. In: Nihoul, J.C.J., Jamart, B.M. (Eds.), Three-Dimensional Models of Marine and Estuarine Dynamics. Elsevier, New York, pp. 405–426.

Sumer, B.M., Jenssen, B.L., Fredsoe, J., 1987. Turbulence in oscillatory boundary layers. In: Compte-Bellot, G., Mathieu, J. (Eds.), Advances in Turbulence. Springer-Verlag, Berlin, pp. 402–425.

Tang, Y.M., Grimshaw, R., 1996. The effect of wind-wave enhancement of bottom stress on the circulation induced by tropical cyclones on continental shelves. Journal of Geophysical Research 101, 22,705–22,714.

Vager, B.G., Kagan, B.A., 1969. The dynamics of the turbulent boundary layer in a tidal current. Izvestiya, Atmospheric and Oceanic Physics 5, 168–179.